Inorganic Chemistry

ARTICLE

pubs.acs.org/IC

The High-Temperature Polymorphs of K_3AlF_6

Graham King,*[,†,‡] Artem M. Abakumov,[§] Patrick M. Woodward,[‡] Anna Llobet,[†] Alexander A. Tsirlin,[∥] Dmitry Batuk,[§] and Evgeny V. Antipov[⊥]

[†]Lujan Neutron Scattering Center, Los Alamos National Laboratory, MS H805, Los Alamos, New Mexico 87545, United States

[‡]Department of Chemistry, The Ohio State University, 100 West 18th Avenue, Columbus, Ohio 43210-1185, United States

[§]Electron Microscopy for Materials Research (EMAT), University of Antwerp, Groenenborgerlaan 171, B-2020 Antwerp, Belgium

[∥]Max Planck Institute for Chemical Physics of Solids, Nöthnitzer Strasse 40, 01187 Dresden, Germany

[⊥]Department of Chemistry, Moscow State University, Moscow 119991, Russia

Supporting Information

ABSTRACT: The crystal structures of the three high-temperature polymorphs of K_3AlF_6 have been solved from neutron powder diffraction, synchrotron X-ray powder diffraction, and electron diffraction data. The β-phase (stable between 132 and 153 °C) and γ-phase (stable between 153 to 306 °C) can be described as unusually complex superstructures of the double-perovskite structure (K_2KAlF_6) which result from noncooperative tilting of the AlF_6 octahedra. The β-phase is tetragonal, space group $I4/m$, with lattice parameters of a = 13.3862(5) Å and c = 8.5617(3) Å (at 143 °C) and Z = 10. In this phase, one-fifth of the AlF_6 octahedra are rotated about the c-axis by ∼45° while the other four-fifths remain untilted. The large ∼45° rotations result in edge sharing between these AlF_6 octahedra and the neighboring K-centered polyhedra, resulting in pentagonal bipyramidal coordination for four-fifths of the K^+ ions that reside on the B-sites of the perovskite structure. The remaining one-fifth of the K^+ ions on the B-sites retain octahedral coordination. The γ-phase is orthorhombic, space group $Fddd$, with lattice parameters of a = 36.1276(4) Å, b = 17.1133(2) Å, and c = 12.0562(1) Å (at 225 °C) and Z = 48. In the γ-phase, one-sixth of the AlF_6 octahedra are randomly rotated about one of two directions by ∼45° while the other five-sixths remain essentially untilted. These rotations result in two-thirds of the K^+ ions on the B-site obtaining 7-fold coordination while the other one-third remain in octahedral coordination. The δ-phase adopts the ideal cubic double-perovskite structure, space group $Fm\bar{3}m$, with a = 8.5943(1) Å at 400 °C. However, pair distribution function analysis shows that locally the δ-phase is quite different from its long-range average crystal structure. The AlF_6 octahedra undergo large-amplitude rotations which are accompanied by off-center displacements of the K^+ ions that occupy the 12-coordinate A-sites.

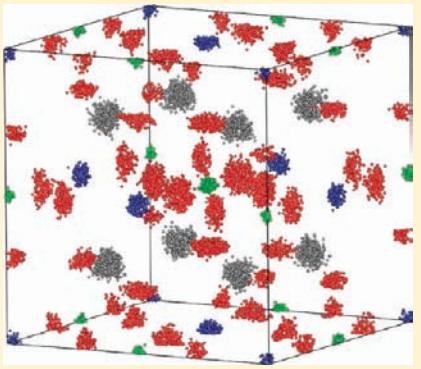

1. INTRODUCTION

Despite its relatively simple chemical formula, the room-temperature crystal structure of K_3AlF_6 is exceptionally complex.[1] It is a member of a rare group of double-perovskite-related compounds which display patterns of noncooperative octahedral tilting. The basic perovskite structure (ABX_3) is based on a three-dimensional network of corner-sharing BX_6 octahedra, with the A-site cations residing in the large cubooctahedral spaces that exist between any eight such BX_6 units. The closely related double-perovskite structure ($A_2BB'X_6$) can be derived from the basic perovskite structure by having two different B-site cations which are ordered in a rock salt pattern, such that each BX_6 unit shares corners with six $B'X_6$ units and vice versa. Octahedral tilting is quite common in perovskites and occurs when the A-site cation is too small to fill the cubooctahedral cavity. When this is the case, the BX_6 octahedra will rotate as nearly rigid units to make shorter A−X bonds while maintaining the ideal B−X bond length. The possible patterns of octahedral tilting are generally assumed to be limited by the corner-sharing connectivity of the octahedral framework, which requires the tilts to act cooperatively.[2] In a few rare cases, such as that of K_3AlF_6, the connectivity of the octahedral framework is broken and the tilting is no longer cooperative. When this occurs, entirely new crystal structures emerge. Such structures tend to be much more complex than those normally adopted by perovskites. Noncooperative octahedral tilting tends to occur in double perovskites which have a very large difference in ionic radii between the B and B′ cations and a relatively small tolerance factor (t = 0.89−0.93).[1] When these criteria are met, some of the smaller $B'X_6$ octahedra undergo ∼45° rotations, which result in these octahedra sharing edges (instead of corners) with the coordination polyhedra of some of the surrounding B cations. This serves to increase the coordination environment of the larger B cations to values greater than 6. Other compounds which are known to display such patterns of noncooperative octahedral tilting include

Received: May 6, 2011
Published: July 11, 2011

Rb_2KCrF_6, Rb_2KGaF_6, $K_3MoO_3F_3$, Sr_3WO_6, Sr_3TeO_6, Ba_3TeO_6, and $A_{11}B_4O_{24}$ (A = Ca, Sr; B = Re, Os; some of the A-sites are vacant).[3−9]

The room-temperature crystal structure of α-K_3AlF_6 is based on the double-perovskite structure (K_2KAlF_6) with K^+ occupying the A-site and K^+ and Al^{3+} rock salt ordered over the B and B′ positions.[1] In this structure all Al^{3+} cations retain a nearly undistorted octahedral coordination by fluorine. Four out of ten of the AlF_6 octahedra undergo large (∼45°) rotations relative to their positions in the ideal double-perovskite structure. One-fifth of the AlF_6 octahedra are rotated about the *c* cubic perovskite subcell axis, while 1/10 are rotated about the *a* cubic perovskite subcell axis and 1/10 are rotated about the *b* cubic perovskite subcell axis. These rotations increase the coordination numbers of the K^+ ions on the B-sites (hereafter denoted K_B) such that now two-fifths are 7-coordinate and three-fifths are 8-coordinate. This pattern of octahedral tilting results in a structure with $Z = 80$ and a unit cell with a volume of over 12 000 Å^3.

A previous study has shown that four polymorphs of K_3AlF_6 exist within the temperature range of 20−800 °C.[10] Upon being heating from room temperature, the α-phase transforms into the *β*-phase. Differential scanning calorimetry (DSC) measurements have shown that the *β*-phase exists within the narrow temperature range of 132−153 °C. It is only observed upon heating, whereas upon cooling the sample appears to undergo a direct $\gamma \rightarrow \alpha$ phase transition at 129 °C. Previous attempts to observe the *β*-phase using X-ray and electron diffraction were not successful, and therefore, no structural information is available on this phase. The previous DSC results have shown that the *γ*-phase exists in the temperature range of 153−306 °C. Electron diffraction experiments have indicated space group *Fddd* and have provided the unit cell dimensions, but the crystal structure has remained unsolved. The X-ray diffraction (XRD) and DSC results indicated that above 300−310 °C K_3AlF_6 transforms into the *δ*-phase.[10−12] The *δ*-phase is reported to have the ideal cubic double-perovskite structure with space group $Fm\bar{3}m$, although atomic coordinates have not yet been reported.[10,12]

The crystal structure of the room-temperature α-phase has already been solved and is described above.[1] In this study, we report the crystal structures of the *β*-, *γ*-, and *δ*-phases of K_3AlF_6 as determined from neutron powder diffraction (NPD), synchrotron X-ray powder diffraction (SXPD), and electron diffraction (ED) measurements. We also show using the pair distribution function (PDF) method that the local structure of the *δ*-phase differs greatly from its cubic long-range average.

2. EXPERIMENTAL SECTION

The synthesis of the K_3AlF_6 sample has been reported elsewhere.[1] The time-of-flight neutron powder diffraction data used for the Rietveld refinements were collected on the high-resolution powder diffractometer (HRPD) of the ISIS facility of the Rutherford Appleton Laboratory. Data sets with long collection times were taken at 143, 225, and 400 °C. In addition, a number of data sets with shorter collection times were taken at 125, 130, 135, 140, 145, 150, 155, 160, and 177 °C. Rietveld refinements were performed using the Topas Academic and JANA2006 software packages.[13,14]

The neutron total scattering data used for the PDF analysis were collected at 400 °C on the neutron powder diffractometer (NPDF) of the Lujan Neutron Scattering Center at Los Alamos National Laboratory. Data reduction to obtain the $G(r)$ function was done using the program PDFgetN.[15] Large box reverse Monte Carlo simulations were done using the program RMCProfile.[16]

Synchrotron X-ray powder diffraction data were collected on the ID31 beamline of the European Synchrotron Radiation Facility (ESRF) ($\lambda = 0.3962$ Å). The data were collected by eight scintillation detectors, each preceded by a Si(111) analyzer crystal, in the angular range $2\theta = 1-40°$. The powder sample was placed into a quartz capillary with an internal diameter of 0.5 mm. To achieve proper statistics and to avoid the preferred orientation, the capillary was spun during the experiment. The sample was heated above room temperature (RT) with a flow of nitrogen or hot air. Data sets with long collection times were taken at 142, 227, and 400 °C. Data sets with shorter collection times were taken as a series of continuous scans in the temperature range from 25 to 375 °C, with the averaged temperatures provided in Table S2 of the Supporting Information. The samples for the ED investigation were prepared by crushing the powder sample in ethanol and depositing it on a holey carbon grid. Selected area ED patterns were recorded using Philips CM20 and Tecnai G2 microscopes equipped with heating holders.

3. RESULTS AND DISCUSSION

3.1. Electron Diffraction: Unit Cells and Space Groups of the *β*- and *γ*-Polymorphs. ED patterns at different temperatures demonstrate a sequence of transformations on going through the $\alpha \rightarrow \beta$ and $\beta \rightarrow \gamma$ phase transitions (Figure 1). The RT ED patterns of the α-phase are indexed according to an $I4_1/a$ tetragonal unit cell, with the lattice vectors related to the basic double-perovskite lattice vectors as $\mathbf{a}_\alpha = 2\mathbf{a}_{dp} - \mathbf{b}_{dp}$, $\mathbf{b}_\alpha = \mathbf{a}_{dp} + 2\mathbf{b}_{dp}$, and $\mathbf{c}_\alpha = 4\mathbf{c}_{dp}$ ($\mathbf{a}_{dp}$, $\mathbf{b}_{dp}$, and $\mathbf{c}_{dp}$ are the basis vectors of the parent double-perovskite cubic unit cell with $a \approx 8.6$ Å).[10] Heating to 150 °C completely suppresses the $4\mathbf{c}_{dp}$ superstructure, but the structure remains tetragonal and the superlattice reflections in the $\mathbf{a}^*-\mathbf{b}^*$ plane stay intact. This set of ED patterns belongs to the *β*-phase and can be indexed with an *I*-centered tetragonal unit cell with $\mathbf{a}_\beta = {}^1/_2\mathbf{a}_{dp} - {}^3/_2\mathbf{b}_{dp}$, $\mathbf{b}_\beta = {}^3/_2\mathbf{a}_{dp} + {}^1/_2\mathbf{b}_{dp}$, and $\mathbf{c}_\beta = \mathbf{c}_{dp}$ ($a_\beta = a_\alpha/\sqrt{2}$; $c_\beta = {}^1/_4c_\alpha$). No other reflection conditions were observed except those imposed by the *I*-centering. The geometry of the [001] ED pattern reflects the absence of 2-fold axes perpendicular to the 4-fold axis and mirror planes parallel to the 4-fold axis. The presence of a 4_1 screw axis is incompatible with $\mathbf{c}_\beta = \mathbf{c}_{dp}$. This restricts the space groups to $I4/m$, $I\bar{4}$, and $I4$. The ED patterns of the *γ*-phase were registered at 190 °C. They are indexed in an orthorhombic unit cell with lattice vectors $\mathbf{a}_\gamma = 3\mathbf{a}_{dp} - 3\mathbf{b}_{dp}$, $\mathbf{b}_\gamma = \mathbf{a}_{dp} + \mathbf{b}_{dp}$, and $\mathbf{c}_\gamma = 2\mathbf{c}_{dp}$ and space group *Fddd*, in agreement with the earlier report.[10]

3.2. High-Temperature NPD and SXPD: Monitoring the Phase Transitions. An overview of the changes in the SXPD patterns of K_3AlF_6 is shown in Figure 2. The SXPD patterns collected between RT and 132 °C can be indexed as the α-phase. The SXPD pattern collected at 137 °C contains peaks corresponding to both the α- and *β*-phases. The SXPD patterns in the 142−152 °C temperature range belong exclusively to the *β*-phase. The $\beta \rightarrow \gamma$ transition occurs over a broad temperature range: SXPD patterns collected between 157 and 172 °C show a mixture of the *β*- and *γ*-phases, while SXPD patterns taken between 177 and 275 °C correspond to the *γ*-phase only. The *γ*-phase transforms to the *δ*-phase at 300 °C. The NPD patterns are in good agreement with the SXPD data (Figure 3). The temperatures of the $\alpha \rightarrow \beta$ and $\beta \rightarrow \gamma$ phase transitions were estimated from NPD data as ∼135 and ∼145−160 °C. The transition temperatures estimated from the SXPD and NPD data are consistent with the previous DSC measurements which show

dx.doi.org/10.1021/ic200956a |*Inorg. Chem.* 2011, 50, 7792–7801

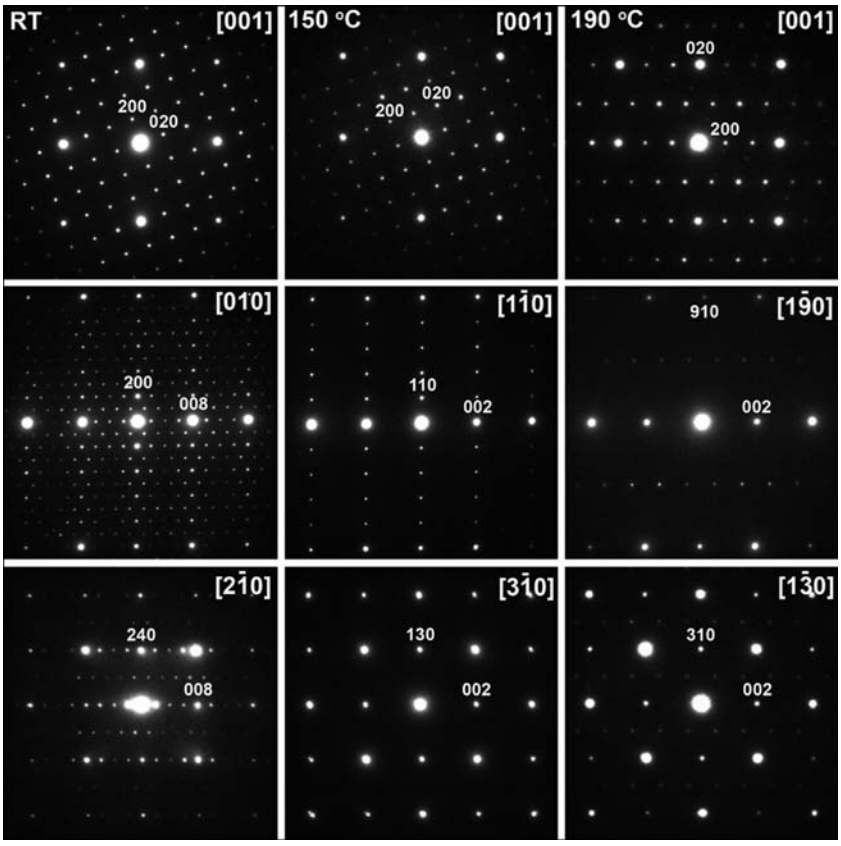

Figure 1. Electron diffraction patterns at RT (α-phase, left column), 150 °C (β-phase, central column), and 190 °C (γ-phase, right column).

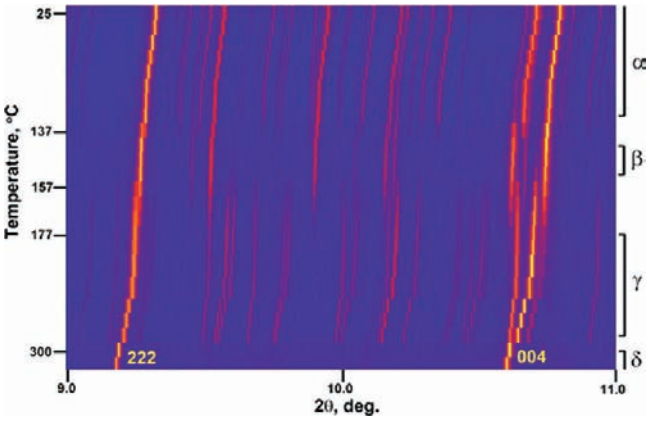

Figure 2. Part of the SXPD patterns showing thermal evolution of the 222 and 004 reflections of the cubic face-centered δ-phase. The stability regions of the four polymorphs are marked. The intensity of the reflections is given in a color code (lowest, blue; highest, yellow). The temperature scale is not linear.

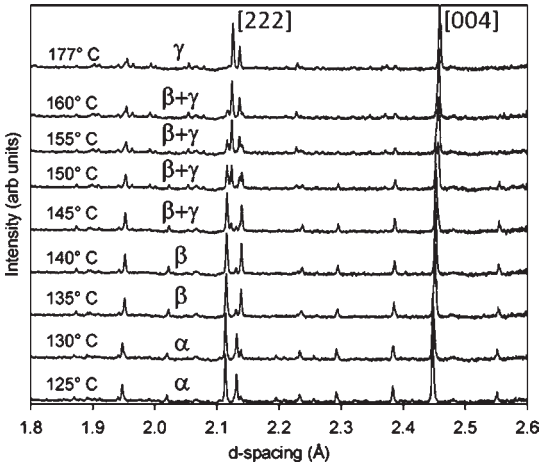

Figure 3. Selected regions of the NPD patterns of K_3AlF_6 at various temperatures showing the $\alpha \rightarrow \beta$ and $\beta \rightarrow \gamma$ phase transitions. The 222 and 004 subcell peak groups have been labeled.

the critical temperatures of the $\alpha \rightarrow \beta$, $\beta \rightarrow \gamma$, and $\gamma \rightarrow \delta$ phase transitions to be 132, 153, and 306 °C, respectively.[10] Lattice parameters obtained by fitting the NPD and SXPD patterns are given in Tables S1 and S2 of the Supporting Information, respectively. Variation of the parameters of the double-perovskite subcell and the subcell volume with temperature for the α-, β-, γ-, and δ-phases are shown in Figure 4. The unit cell parameters and volume demonstrate clear discontinuities at the phase transitions. This, together with the observation of the coexistence of the low- and high-temperature phases at the $\alpha \rightarrow \beta$ and $\beta \rightarrow \gamma$ phase transitions, indicates that all transitions are of first order.

3.3. Crystal Structure of the *β*-Phase. The unit cell of the β-phase is the same as the unit cells of the related compounds Rb_2KCrF_6 and Rb_2KGaF_6 (after transformation from the non-standard *F*-centered unit cell to the standard *I*-centered cell).[3] The crystal structures of these compounds were therefore used as a starting point for the refinement of the β-phase crystal structure. Rietveld refinements were done in space groups *I*4/*m*,

dx.doi.org/10.1021/ic200956a |*Inorg. Chem.* 2011, 50, 7792–7801

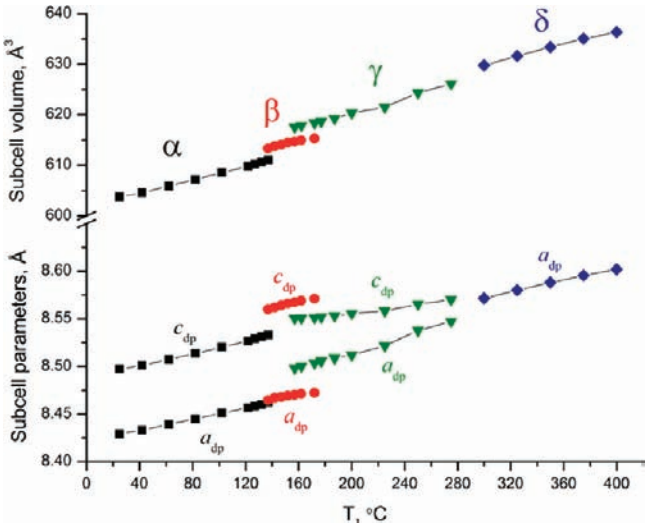

Figure 4. Temperature variation of the double-perovskite subcell parameters and subcell volume for the four polymorphs. For the α- and β-phases the subcell is tetragonally distorted. The subcell of the γ-phase has $a_{dp} = b_{dp}$ and is slightly monoclinically distorted with the monoclinic angle $\gamma \approx 90.07°$.

$I\bar{4}$, and $I4$. A satisfactory fit to the peak intensities could be obtained using space group $I4/m$. Refinements using an $I\bar{4}$ model gave a distinctly worse fit and negative atomic displacement parameters (ADPs) for the Al atoms, so this model was discarded. Refinements in space group $I4$ provided a small improvement to the fit and allowed for a small amount of additional octahedral tilting. While it is not possible to conclusively differentiate between $I4/m$ and $I4$, it is apparent that any deviations from $I4/m$ symmetry, if they exist, are subtle. Therefore, the results of the $I4/m$ refinement are given. The refinement was done jointly against both the NPD pattern taken at 143 °C and the SXPD pattern taken at 142 °C, with both patterns weighted equally. The r_{wp} of the fit to the SXPD data was 10.7, and the r_{wp} of the fit to the NPD data was 8.0. The ADPs of all atoms corresponding to the same type of position (K_A, K_B, Al, and F) were constrained to be the same. Experimental, calculated, and difference SXPD and NPD profiles after the Rietveld refinement are shown in Figure 5. Crystallographic data are given in Table 1. The atomic coordinates are given in Table 2, and selected bond distances are given in Table 3.

The crystal structure of β-K_3AlF_6 can be described as a derivative of the double-perovskite structure. The key difference is large (~45°) rotations about the c-axis of one-fifth of the AlF_6 octahedra. The other octahedra have the positions they would have in the ideal double-perovskite structure. The ~45° rotations result in four-fifths of the K_B atoms obtaining a 7-coordinate pentagonal-bipyramidal geometry while the remaining one-fifth retain octahedral coordination (Figure 6). The F atoms of the common edge of the heavily rotated AlF_6 octahedron and K_BF_7 polyhedron form particularly long bonds to the K_B atoms. In response, these K_B atoms undergo large displacements of ~0.48 Å from their ideal positions toward the edge shared with the AlF_6 octahedra.

Bond valence sums (BVSs) were calculated for all of the cations. According to Brown et al., the R_0 constant in the BVS equation as estimated from the room-temperature bond lengths cannot be directly used for calculating BVSs at higher

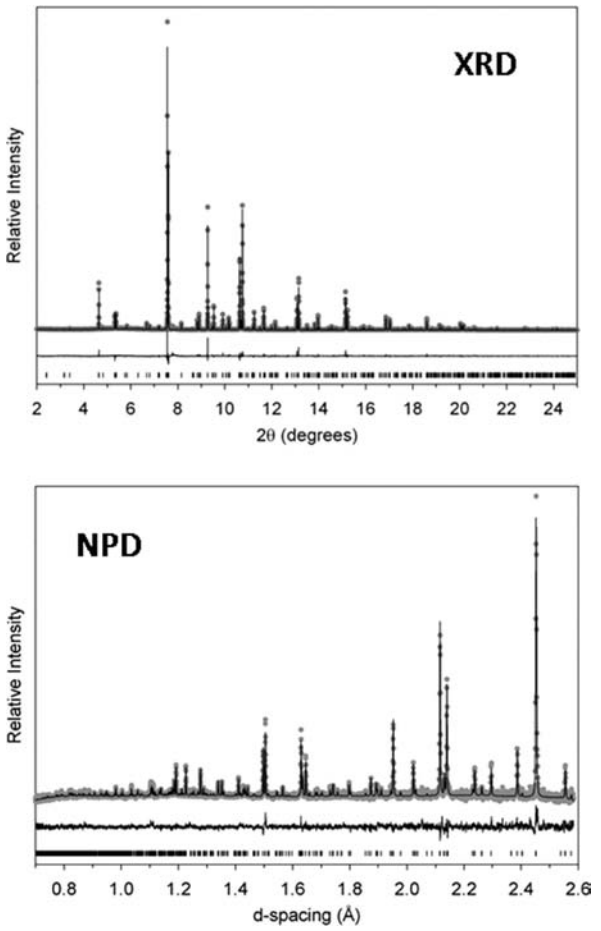

Figure 5. Results of the joint Rietveld refinement of the XRD and NPD patterns of β-K_3AlF_6. The gray circles are the data points, the solid line is the fit, the difference curve is shown beneath, and the tick marks show the positions of allowed *hkl* reflections.

Table 1. Crystallographic Data for the Four Polymorphs of K_3AlF_6[a]

	α-phase	β-phase	γ-phase	δ-phase
temp (°C)	25	143	225	400
space group	$I4_1/a$	$I4/m$	$Fddd$	$Fm\bar{3}m$
a (Å)	18.8385(3)	13.3862(5)	36.1276(4)	8.5943(1)
b (Å)			12.0562(1)	
c (Å)	33.9644(6)	8.5617(3)	17.1133(2)	
V (Å^3)	12,053.6(3)	1,534.2(2)	7,453.9(3)	634.79(1)
Z	80	10	48	4
density (g/cm^3)	2.845	2.801	2.761	2.702

[a] The data for the α-phase were taken from ref 1.

temperatures.[17,18] The R_0 value as a function of temperature can be calculated as $R_0(T) = R_0 + (dR/dT)\Delta T$, where dR/dT is a function of the bond valence s and ΔT is the temperature increase with respect to room temperature.[18] For the Al−F bond with a length of 1.81 Å, $dR/dT \approx 2 \times 10^{-5}$ Å·K^{-1} (see Figure 5 in ref 18). For the maximal temperature of 400 °C used in this investigation, this gives only a ~0.5% increase of R_0 and a ~2% increase in the bond valence. These changes are comparable with those caused by experimental

dx.doi.org/10.1021/ic200956a |*Inorg. Chem.* 2011, 50, 7792–7801

Table 2. Atomic Coordinates and Displacement Parameters for β-K_3AlF_6 at ~143 °C from the Joint Rietveld Refinement of the NPD Pattern and SXPD Patterns

atom	Wyckoff site	x/a	y/b	z/c	U_{iso} (Å^2)
$K_A(1)$	4*d*	0	1/2	1/4	0.0440(4)
$K_A(2)$	16*i*	0.1069(1)	0.2097(1)	0.2698(2)	0.0440(4)
$K_B(1)$	2*b*	0	0	1/2	0.0625(7)
$K_B(2)$	8*h*	0.2316(2)	0.4178(2)	1/2	0.0625(7)
Al(1)	2*a*	0	0	0	0.0179(5)
Al(2)	8*h*	0.1995(2)	0.3989(3)	0	0.0179(5)
F(1)	8*h*	0.0653(6)	0.1189(5)	0	0.0633(5)
F(2)	4*e*	0	0	0.2110(9)	0.0633(5)
F(3)	8*h*	0.3260(5)	0.4493(7)	0	0.0633(5)
F(4)	8*h*	0.1529(7)	0.5382(5)	0	0.0633(5)
F(5)	8*h*	0.0759(5)	0.3660(7)	0	0.0633(5)
F(6)	8*h*	0.2446(8)	0.2779(5)	0	0.0633(5)
F(7)	16*i*	0.2021(3)	0.4074(3)	0.2047(4)	0.0633(5)

Table 3. Selected Interatomic Distances for β-K_3AlF_6 (Å)

Al(1)−F(1)	1.816(7) × 4	$K_A(1)$−F(4)	3.005(7) × 4
Al(1)−F(2)	1.806(9) × 2	$K_A(1)$−F(5)	2.972(6) × 4
Al(2)−F(3)	1.823(8)	$K_A(1)$−F(7)	3.001(4) × 4
Al(2)−F(4)	1.967(8)	$K_A(2)$−F(1)	2.669(4)
Al(2)−F(5)	1.712(8)	$K_A(2)$−F(2)	3.191(2)
Al(2)−F(6)	1.728(8)	$K_A(2)$−F(3)	3.036(7)
Al(2)−F(7)	1.757(3) × 2	$K_A(2)$−F(3)	2.927(7)
$K_B(1)$−F(2)	2.475(9) × 2	$K_A(2)$−F(4)	2.848(7)
$K_B(1)$−F(3)	2.426(7) × 4	$K_A(2)$−F(5)	3.144(7)
$K_B(2)$−F(1)	2.763(9)	$K_A(2)$−F(6)	3.093(7)
$K_B(2)$−F(1)	2.811(8)	$K_A(2)$−F(6)	2.804(8)
$K_B(2)$−F(4)	2.756(8)	$K_A(2)$−F(7)	2.989(4)
$K_B(2)$−F(5)	2.487(8)	$K_A(2)$−F(7)	3.007(4)
$K_B(2)$−F(6)	2.638(7)	$K_A(2)$−F(7)	2.928(4)
$K_B(2)$−F(7)	2.563(3) × 2		

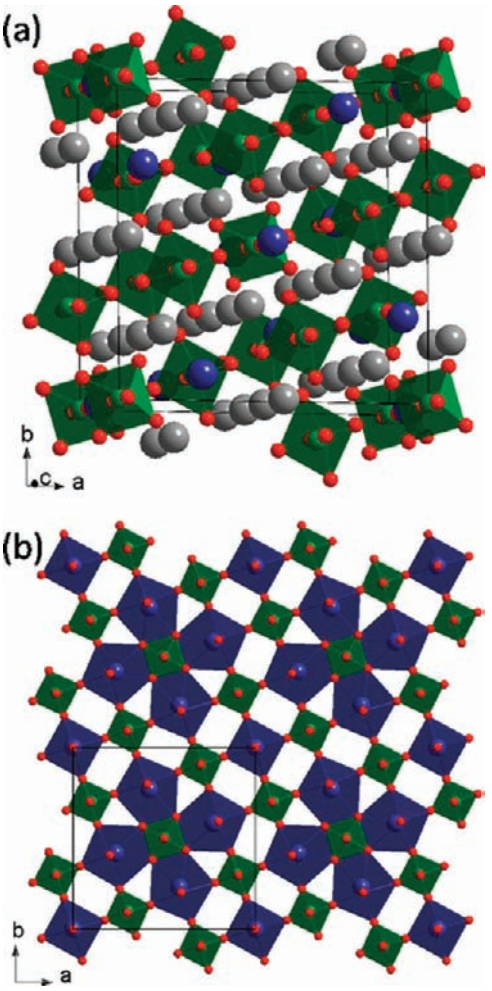

Figure 6. Two views of the crystal structure of β-K_3AlF_6. (a) shows a single unit cell. The small green atoms are Al, the large blue atoms are K_B, the large gray atoms are K_A, and the small red atoms are F. The lines show the unit cell boundaries. (b) shows a single layer of Al and K_B coordination polyhedra viewed down the *c*-axis.

uncertainties in the bond lengths and will be ignored in further BVS calculations.

The Al(1) and Al(2) atoms have BVSs of 2.91 and 3.17, which are in good agreement with their expected valence of 3. The $K_B(1)$ atom, which is in octahedral coordination, has a BVS of 1.78, showing it to be strongly overbonded. The $K_B(2)$ atom, which is in pentagonal-bipyramidal geometry, has a BVS of 1.22, which is much closer to its ideal valence of 1. However, this atom is still distinctly overbonded. The large degree of overbonding for the K_B atoms may be responsible for the apparent instability of the β-phase. The K atoms that reside on the A-site (K_A) have BVSs that are fairly close to their ideal values, although there is a small degree of underbonding. The BVSs for the $K_A(1)$ and $K_A(2)$ atoms are 0.80 and 0.86, respectively.

The crystal structure of β-K_3AlF_6 is isostructural with the low-temperature crystal structures of Rb_2KCrF_6 and Rb_2KGaF_6.[3] The β-phase of K_3AlF_6 is also closely related to the α-phase of K_3AlF_6. In both crystal structures one-fifth of the AlF_6 octahedra are rotated by ~45° about the *c*-axis. The α → β phase transition can be thought to primarily involve the AlF_6 octahedra which are rotated by ~45° about the *a* and *b* subcell axes in the α-phase. During the transition, these octahedra rotate back to their original positions in the ideal double-perovskite structure. The changes in the orientations of these octahedra appear to expand the structure along the *c*-axis. As can be seen in Figure 4, there is a discontinuous increase in the c_{dp} subcell parameter upon passing through the phase transition. Meanwhile, the a_{dp} subcell parameter increases smoothly, seemingly unaffected by the phase transition.

3.4. Crystal Structure of the γ-Phase. In constructing a starting model for the refinement of the γ-phase, several simplifying assumptions were made. First, it was assumed that the cation sublattice remains essentially the same as in the double-perovskite structure. It was also assumed that the Al cations retain octahedral coordination by fluorine but the K_B cations do not necessarily have octahedral coordination. The initial positions for all atoms were the positions they would have in the ideal double-perovskite structure. When the cubic structure is transformed into the *Fddd* supercell, there are two possible choices of origin which place the B and B′ cations on sites with different symmetries. One possibility is to have four B cations: two residing on the 8*a* and 8*b* Wyckoff sites and two others residing on 16*e* sites. In this setting, there are two B′ cations which sit on

dx.doi.org/10.1021/ic200956a |*Inorg. Chem.* 2011, 50, 7792–7801

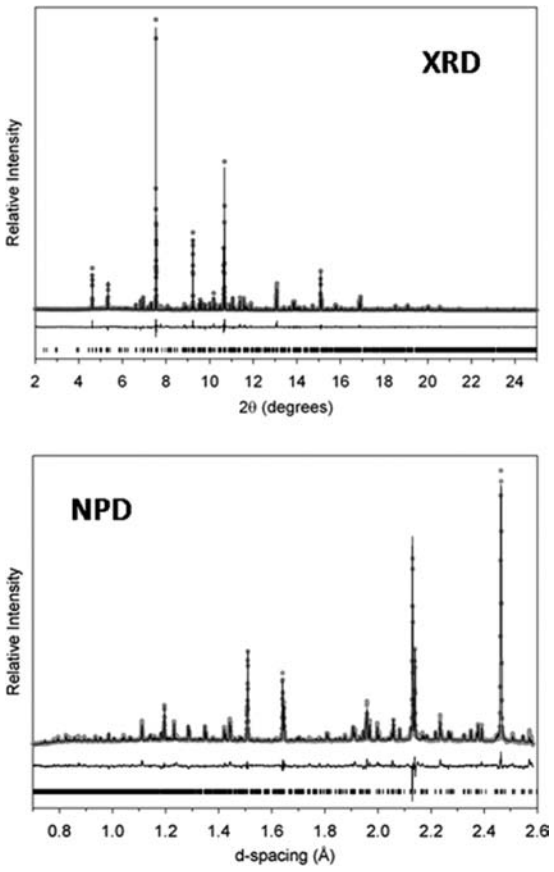

Figure 7. Results of the joint Rietveld refinement of the XRD and NPD patterns of γ-K_3AlF_6. The gray circles are the data points, the solid line is the fit, the difference curve is shown beneath, and the tick marks show the positions of allowed *hkl* reflections.

16*g* and 32*h* sites. The other origin choice has the B and B′ cations reversed.

Refinements were done jointly against the NPD and SXPD data sets using both origin choices with rigid-body constraints for the AlF_6 octahedra to reduce the number of variables during the early stages of refinement. During the final stages of the refinement, all constraints were removed and displacement parameters were allowed to refine. Despite the large number of structural variables (41 degrees of freedom for the atomic positions), good fits to the data could not be obtained using either model. After having exhaustively searched for a solution in space group *Fddd*, symmetry lowering was considered. Two models were found in space groups *Fdd*2 and *F*2*dd* which fit the data equally well. Both models are structurally very similar, and each has one-sixth of the AlF_6 octahedra undergoing large rotations while the remaining five-sixths remain essentially untilted and undistorted. This suggested that having one-sixth of the octahedra heavily rotated could be a key structural feature of this phase. In both models, the rotated octahedron was strongly distorted, resulting in unreasonably short F−F distances. The fact that equivalent good fits with nearly the same structure could be obtained with *d*-glide planes perpendicular to either the *a*- or *c*-axis suggests that both glide planes are present and the true symmetry is indeed *Fddd*. The large distortion of the rotated octahedra can be taken as a sign that there is positional disorder of the F atoms that are part of these octahedra. On the basis of this knowledge, a new model

Table 4. Atomic Coordinates, Site Occupancies (Occ), and Displacement Parameters for γ-K_3AlF_6 at ∼225 °C from the Joint Rietveld Refinement of the NPD and SXPD Patterns

atom	Wyckoff site	*x*/*a*	*y*/*b*	*z*/*c*	Occ	U_{iso} (Å^2)
Al(1)	8*a*	1/8	1/8	1/8	1	0.0102(5)
Al(2)	8*b*	1/8	5/8	1/8	1	0.0102(5)
Al(3)	16*e*	0.2892(2)	1/8	1/8	1	0.0102(5)
Al(4)	16*e*	0.4581(2)	1/8	1/8	1	0.0102(5)
K_B(1)	32*h*	0.1979(1)	0.3965(3)	0.1258(2)	1	0.0389(5)
K_B(2)	16*g*	1/8	1/8	0.4127(3)	1	0.0389(5)
K_A(1)	32*h*	0.1247(1)	0.3442(3)	0.2642(2)	1	0.0389(5)
K_A(2)	32*h*	0.2102(1)	0.1210(4)	0.2504(2)	1	0.0389(5)
K_A(3)	32*h*	0.2159(1)	0.1283(4)	0.7619(2)	1	0.0389(5)
F(1)	32*h*	0.1575(1)	0.0175(5)	0.1199(4)	1	0.0428(5)
F(2)	16*g*	1/8	1/8	0.2314(4)	1	0.0428(5)
F(3)	32*h*	0.1545(3)	0.5679(9)	0.1934(6)	0.5	0.0428(5)
F(4a)	32*h*	0.0815(3)	0.5614(8)	0.1559(6)	0.5	0.0428(5)
F(4b)	32*h*	0.1311(3)	0.7401(8)	0.1939(5)	0.5	0.0428(5)
F(5)	32*h*	0.2901(2)	0.1203(6)	0.0206(3)	1	0.0428(5)
F(6)	32*h*	0.2544(2)	0.2311(4)	0.1253(5)	1	0.0428(5)
F(7)	32*h*	0.3240(2)	0.0162(5)	0.1249(5)	1	0.0428(5)
F(8)	32*h*	0.4594(2)	0.1382(5)	0.0217(3)	1	0.0428(5)
F(9)	32*h*	0.4925(2)	0.2361(5)	0.1270(5)	1	0.0428(5)
F(10)	32*h*	0.4242(2)	0.0178(5)	0.1230(5)	1	0.0428(5)

was constructed with *Fddd* symmetry. The origin choice which has the Al cations on the 8*a*, 8*b*, and two 16*e* sites was chosen, since this permits one-sixth of the octahedra to be unique. The F atoms surrounding the Al on site 8*b* were split into two positions. The F3 atom (on site 16*g*) was moved onto a general position with 32-fold multiplicity. The F4 atom, which was already on a general position, was split into two atoms (F4a and F4b). The F3, F4a, and F4b atoms were all given site occupancies equal to one-half. This increased the total number of atomic degrees of freedom to 46. It should be noted that without split positions it is not possible to have one-sixth of the AlF_6 octahedra with a unique rotation angle in space group *Fddd* since the symmetry of the 8-fold sites prohibits these octahedra from rotating. This model provided an excellent fit to both the SXPD and NPD diffraction patterns (Figure 7). The r_{wp} of the fit to the XRD data was 10.0, and the r_{wp} of the fit to the NPD data was 2.86. Crystallographic data for γ-K_3AlF_6 are given it Table 1. The atomic coordinates are given in Table 4, and selected bond distances are given in Table 5.

The crystal structure of γ-K_3AlF_6 is shown in Figures 8 and 9. It can be described as a superstructure of the double-perovskite structure where one-sixth of the AlF_6 octahedra are rotated by ∼45° while the other five-sixths of the AlF_6 octahedra remain nearly untilted and undistorted. These large rotations are disordered and randomly occur about either the [110] or [$\bar{1}$10] direction (corresponding to the a_{dp} or b_{dp} subcell axes). The disorder could be related to the weak interaction between the rotated octahedra due to the large separation between them. A large rotation in one of these two directions is probably needed to stabilize the structure, but since the rotated octahedra are far apart, it makes little energy difference in which direction this rotation occurs relative to the other rotated octahedra. Disordered anion positions in double-perovskite-related compounds

dx.doi.org/10.1021/ic200956a |*Inorg. Chem.* 2011, 50, 7792–7801

Table 5. Selected Interatomic Distances for γ-K_3AlF_6 (Å)

Al(1)−F(1)	1.751(6) × 4	K_A(1)−F(1)	3.044(7)
Al(1)−F(2)	1.821(7) × 2	K_A(1)−F(8)	3.069(8)
Al(2)−F(3)	1.73(1) × 4	K_A(1)−F(10)	3.072(8)
Al(2)−F(4a)	1.83(1) × 4	K_A(1)−F(5)	3.088(8)
Al(2)−F(4b)	1.83(1) × 4	K_A(1)−F(7)	3.126(8)
Al(3)−F(5)	1.788(5) × 2	K_A(1)−F(3)	3.15(1)
Al(3)−F(6)	1.795(7) × 2	K_A(2)−F(5)	2.911(7)
Al(3)−F(7)	1.816(7) × 2	K_A(2)−F(8)	2.926(8)
Al(4)−F(8)	1.776(5) × 2	K_A(2)−F(6)	2.949(8)
Al(4)−F(9)	1.827(7) × 2	K_A(2)−F(7)	2.969(9)
Al(4)−F(10)	1.779(7) × 2	K_A(2)−F(6)	2.983(8)
K_B(1)−F(4a)	2.32(1)	K_A(2)−F(9)	3.004(9)
K_B(1)−F(1)	2.460(7)	K_A(2)−F(6)	3.009(8)
K_B(1)−F(5)	2.550(6)	K_A(2)−F(5)	3.042(9)
K_B(1)−F(8)	2.565(6)	K_A(2)−F(10)	3.084(9)
K_B(1)−F(9)	2.577(6)	K_A(2)−F(2)	3.094(4)
K_B(1)−F(3)	2.84(1)	K_A(2)−F(1)	3.109(7)
K_B(1)−F(6)	2.853(6)	K_A(2)−F(1)	3.188(7)
K_B(1)−F(4b)	3.02(1)	K_A(3)−F(4a)	2.60(1)
K_B(2)−F(10)	2.550(6) × 2	K_A(3)−F(3)	2.61(1)
K_B(2)−F(7)	2.590(6) × 2	K_A(3)−F(9)	2.734(8)
K_B(2)−F(3)	2.77(1) × 2	K_A(3)−F(8)	2.763(7)
K_B(2)−F(4b)	2.83(1) × 2	K_A(3)−F(6)	2.785(8)
K_B(2)−F(2)	3.102(8) × 2	K_A(3)−F(5)	2.929(9)
K_A(1)−F(4b)	2.34(1)	K_A(3)−F(7)	2.930(8)
K_A(1)−F(2)	2.702(4)	K_A(3)−F(10)	2.998(8)
K_A(1)−F(10)	2.790(8)	K_A(3)−F(9)	3.081(8)
K_A(1)−F(7)	2.800(8)	K_A(3)−F(9)	3.098(9)
K_A(1)−F(1)	2.914(7)	K_A(3)−F(8)	3.226(8)

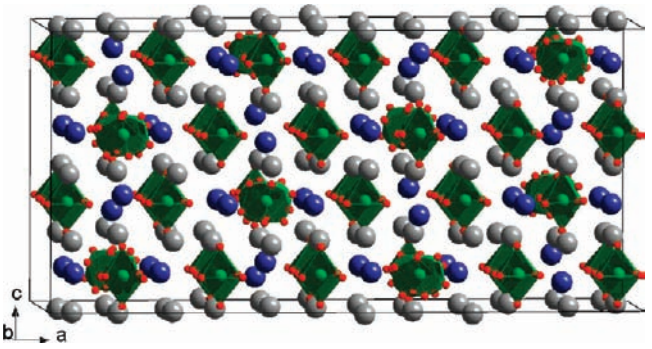

Figure 8. One unit cell of γ-K_3AlF_6. The color scheme is the same as for Figure 4.

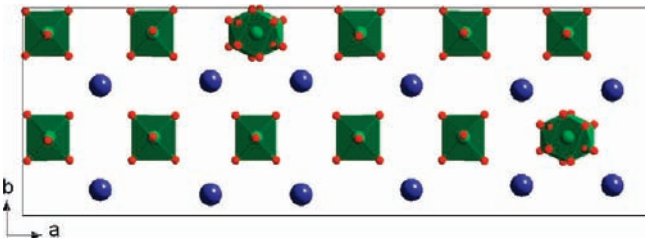

Figure 9. A single layer of AlF_6 octahedra and K_B atoms in γ-K_3AlF_6 viewed down the *c*-axis. The color scheme is the same as for Figure 4.

with a large B/B′ size difference have been observed before, such as in the case of $Ba_{11}W_4O_{23}$.[19] Bond valence sums for the Al(1), Al(2), Al(3), and Al(4) cations were calculated to be 3.24, 3.08, 3.02, and 3.07, respectively, in good agreement with their expected values.

The large ∼45° rotations of the AlF_6 octahedra serve to increase the coordination numbers of some of the B-site cations. A large ∼45° rotation of an AlF_6 octahedron will result in edge sharing between the AlF_6 octahedron and the coordination polyhedra of four out of six neighboring B-site cations. In γ-K_3AlF_6, every K_B atom is surrounded by one heavily tilted AlF_6 octahedron and five nearly untilted octahedra. Edge sharing will occur if the rotation axis is perpendicular to the vector connecting the Al and K_B atoms. If this vector coincides with the rotation axis, corner sharing persists. There are two crystallographically unique K_B atoms in γ-K_3AlF_6, the K_B(1) atom on Wyckoff position 32*h* and the K_B(2) atom on Wyckoff position 16*g*. Due to the disorder in the direction of the octahedral tilting, half of the K_B(1) atoms become 7-coordinated while the other half retain a 6-coordinated octahedral environment. The BVS for K_B(1) is 1.31, indicating that this atom is somewhat overbonded. It could be expected that the K_B(1) atoms which are 7-coordinated are able to obtain a BVS which is close the ideal value while the overbonding is more severe for those that are 6-coordinated. The K_B(2) atoms are always 7-coordinated and have a BVS of 1.12, which is much closer to the ideal valence. There is still disorder in the way the K_B(2) atom is coordinated by the F atoms on the heavily rotated octahedron, but whichever way this octahedron is rotated, edge sharing results. Depending on the direction the AlF_6 octahedron is rotated, the shared edge runs along one of two perpendicular directions.

As discussed earlier, edge sharing results in two long bonds between F atoms belonging to the heavily rotated AlF_6 octahedron and the K_B atoms. This causes the K_B atoms to shift toward the edge shared with the rotated AlF_6 octahedron. The K_B(1) atom is found to shift about 0.42 Å, while the K_B(2) atom shifts about 0.64 Å. The smaller apparent shift of the K_B(1) atom is probably related to the fact that, due to the disorder of the F atom positions, only half of these atoms share an edge of their coordination polyhedron with an AlF_6 octahedron. When the edge sharing occurs, those K_B(1) atoms may be shifted by a distance which is very similar to what the K_B(2) atoms are shifted by, whereas those K_B(1) atoms that do not share an edge with a neighboring AlF_6 octahedron undergo only small displacements. The shift observed in the crystal structure would be an average of these two situations. The large ADPs obtained for the K atoms suggest that a small degree of positional disorder may exist for the K atoms, which is most likely caused by the disorder in the F positions.

The large rotation of one-sixth of the AlF_6 octahedra also changes the coordination environments of some of the K_A atoms. In the double-perovskite structure, each A-site cation is neighbored by four B and four B′ cations. There are three crystallographically unique K_A atoms in γ-K_3AlF_6. The K_A(1) and K_A(3) atoms are each surrounded by three nearly untilted AlF_6 octahedra and one heavily tilted AlF_6 octahedron. This tilting reduces their coordination number below 12 and allows for the formation of some shorter K−F bonds. The BVSs for the K_A(1) and K_A(3) atoms are 0.94 and 0.93, respectively, showing that they have a nearly ideal coordination environment. The K_A(2) atom is surrounded by nearly untilted AlF_6 octahedra only and therefore retains a nearly undistorted cubooctahedral coordination environment. The BVS of the K_A(2) atom is calculated to be 0.76, which shows that the lack of octahedral tilting around it leaves this atom underbonded.

dx.doi.org/10.1021/ic200956a |*Inorg. Chem.* 2011, 50, 7792–7801

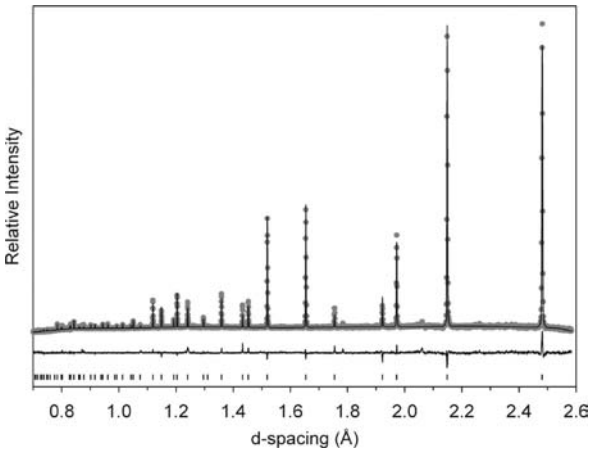

Figure 10. Results of the Rietveld refinement of the NPD pattern of δ-K_3AlF_6. The gray circles are the data points, the solid line is the fit, the difference curve is shown beneath, and the tick marks show the positions of allowed *hkl* reflections.

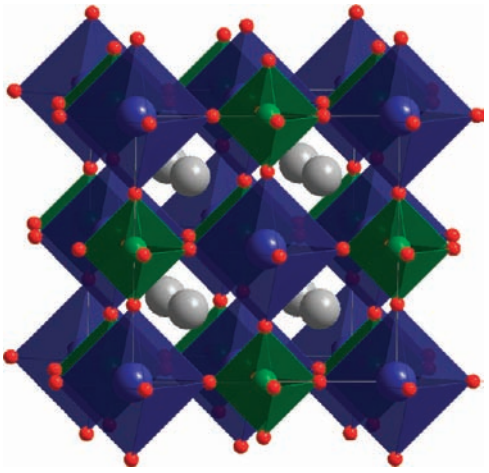

Figure 11. Crystal structure of δ-K_3AlF_6. The color scheme is the same as for Figure 4.

3.5. Crystal Structure and Local Structure of the δ-Phase.

A previous study has reported that above 306 °C the crystal structure of K_3AlF_6 transforms into that of the ideal cubic double perovskite with space group $Fm\bar{3}m$.[10] Our SXPD data show that the $\gamma \rightarrow \delta$ transition occurs between 275 and 300 °C. The NPD and SXPD patterns collected at 400 °C can be indexed using space group $Fm\bar{3}m$. A Rietveld refinement using the NPD data was carried out in this space group to determine the structural parameters. The only structural variables to refine in $Fm\bar{3}m$ are the *x* position of the F site and the four atomic displacement parameters. Refinement of these variables was not able to produce a satisfactory fit to all peak intensities. Refinement of anisotropic ADPs for the F atom improved the fit significantly and resulted in all peak intensities being reasonably well fit (Figure 10). The refinement had an r_{wp} of 2.49. The resulting structure is shown in Figure 11. Crystallographic data are given in Table 1, and the atomic coordinates are given in Table 6. A Rietveld refinement of the 400 °C SXPD data (Figure S1, Supporting Information) produced nearly identical results.

Table 6. Atomic Coordinates and ADPs for δ-K_3AlF_6 from Rietveld Refinement of the 400 °C NPD Pattern

atom	Wyckoff site	*x*/*a*	*y*/*b*	*z*/*c*	ADP, Å^2
K_A	8*c*	1/4	1/4	1/4	U_{iso} = 0.0654(1)
K_B	4*a*	0	0	0	U_{iso} = 0.0505(1)
Al	4*b*	1/2	1/2	1/2	U_{iso} = 0.0243(1)
F	24*e*	0.29085(1)	0	0	U_{11} = 0.0292(1)
					$U_{22} = U_{33}$ = 0.1126(2)

The anisotropy of the ADPs for the F atom is quite large. The fluorine mean square displacements perpendicular to the Al−F and K_B−F bonds were refined to be about 4 times larger than the displacements parallel to these bonds. This suggested the possibility that large-amplitude dynamic rotations of the AlF_6 octahedra are occurring in this phase. Additional Rietveld refinements were carried out where the AlF_6 octahedron was defined as a rigid body and the TLS definition was used for the displacement parameters. The TLS method defines the displacements of the atoms in terms of translations, librations, and screw motions of the entire rigid body. The advantage of using the TLS definition in this particular case is that the average rotation of the AlF_6 octahedron is given in units of degrees. These refinements showed that the average rotational displacement of the AlF_6 octahedron is 9.7(1)°.

The bond distances in the crystal structure of δ-K_3AlF_6 as obtained from the Rietveld refinements were also unusual. The Al−F distance of 1.798(1) Å is slightly shorter than expected considering the average Al−F distance at room temperature is 1.81 Å.1 The K_B−F bond length was refined to be 2.500(1) Å, which is much shorter than expected and gives a bond valence sum for the K_B atom of 1.52. The K_A−F bond length was refined to be 3.0588(1) Å, which leaves this atom severely underbonded with a BVS of only 0.67. The large deviation of the BVS parameters of all the K atoms from their ideal valence of 1 would seem to suggest that the δ-phase should be unstable. One possible explanation for these observations is that there are large local deviations from the average structure which relieve these bonding instabilities. Disorder of the F atoms has been reported in the related compound Na_3AlF_6.[20] To test this hypothesis and gain further information about the local structure of this phase, a pair distribution function analysis was carried out on the δ-phase.

To see if the local structure differs significantly from the long-range average structure, the low *r* region of the experimental $G(r)$ function was fit using the average cubic structure as a model. The resulting fit is extremely poor (Figure S2, Supporting Information), showing that large local distortions do exist. To model $G(r)$, large box reverse Monte Carlo (RMC) simulations were performed using the RMCProfile program. A 7 × 7 × 7 supercell of the crystallographic unit cell was constructed which contained 13 720 atoms. The initial positions for the atoms were their positions in the average structure. The refinement was done jointly against both the $G(r)$ and $S(Q)$ functions. The final fit is shown in the Supporting Information as Figure S3.

One way to visualize the results of the RMC refinement is to fold the supercell back into a single unit cell so that "clouds" of atom spatial distributions can be seen. The folded supercell of δ-K_3AlF_6 is shown in Figure 12. The Al distribution is small and spherical and can be fully accounted for by the thermal vibrations of the Al atoms around their average position, indicating that

dx.doi.org/10.1021/ic200956a |*Inorg. Chem.* 2011, 50, 7792–7801

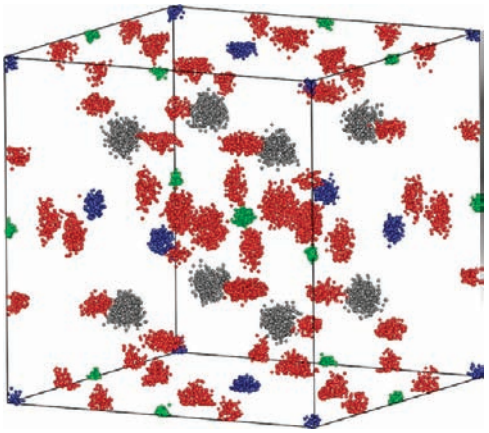

Figure 12. Final configuration of the RMC supercell of δ-K_3AlF_6 folded back into a single unit cell. The green dots are Al atoms, the blue dots are K_B atoms, the gray dots are K_A atoms, and the red dots are F atoms.

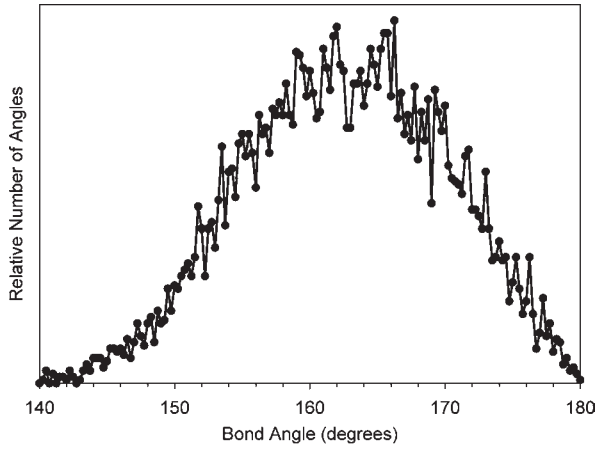

Figure 13. Distribution of Al−F−K_B bond angles in δ-K_3AlF_6 extracted from the RMC configuration.

there is no local disorder of these atoms. The spatial distribution of the K_B atoms is also spherical but slightly broader than the distribution of the Al atoms, showing a small degree of disorder. The K_A atoms show a very broad spatial distribution that is also spherical. This very broad distribution is consistent with the larger than normal ADP obtained for this atom from the Rietveld refinement. Close inspection of the K_A distribution reveals that these atoms do not tend to lie exactly on the A-site, but rather undergo off-center displacements.

The RMC results also show that the spatial distribution of F atoms is highly anisotropic. The distribution is quite narrow in the direction parallel to the Al−F and K_B−F bonds but very broad perpendicular to these bonds. This would seem to indicate that the AlF_6 octahedra undergo significant rotations. To more quantitatively understand the nature of these rotations, the distribution of Al−F−K_B angles was extracted from the RMC configuration (Figure 13). The average Al−F−K_B angle in the configuration is 162.5°. This corresponds to a rotation of the AlF_6 octahedral unit by 10.2°, which is in good agreement with the result obtained from the TLS Rietveld refinement. One important observation is that there are essentially no Al−F−K_B bond angles at or near 180°, meaning that the F atoms almost never lie on their average position. The most likely explanation for these observations is that the AlF_6 octahedra in the δ-phase are undergoing dynamic rotations within a bimodal potential energy well. The potential energy minimum occurs when the octahedral rotation angle is ~10°, and the linear 180° Al−F−K_B configuration (0° tilt) represents a local maximum.

The RMC results give more reasonable average bond lengths than were obtained from the Rietveld refinements. The large rotations of the AlF_6 ocahedra allow for longer Al−F and K_B−F bond lengths. The average Al−F bond length in the RMC configuration is 1.826 Å, which is 0.028 Å longer than that obtained from the Rietveld refinement and represents a slight elongation relative to that of the room-temperature structure. The average K_B−F bond length of 2.532 Å is 0.032 Å longer than in the average structure and results in the overbonding of the K_B atom being less severe than it appears to be from the average structure. The octahedral rotations and off-center displacements of the K_A atoms result in a broad distribution of K_A−F bond lengths and serve to relieve the underbonding of this atom. It could be expected that the direction of the K_A displacements is dictated by the local instantaneous arrangement of octahedral tilts.

The observation of dynamic rotations of the AlF_6 octahedra in δ-K_3AlF_6 raises the possibility that such rotations could be occurring in some of the lower temperature phases as well. The $\alpha \rightarrow \beta$ phase transition involves some heavily tilted octahedra transforming to an untilted configuration. If these octahedra are not simply changing orientation but are also beginning to undergo dynamic rotations, it could mean that some of the apparent overbonding and underbonding of the K atoms in this phase is not as severe as it appears to be. The $\beta \rightarrow \gamma$ phase transition involves a more significant rearrangement of the structure where the distribution of the heavily tilted octahedra changes. It is likely that in this phase some or all of the untilted octahedra undergo large-amplitude dynamic rotations as well. The existence of large-amplitude dynamic rotations in the β- and γ-phases is supported by the large values of the F atom ADPs obtained from the Rietveld refinements.

There are a few other double perovskites which display noncooperative octahedral tilting at lower temperature but transform into a cubic phase at higher temperature, such as Rb_2KCrF_6, Rb_2KGaF_6, and Sr_3WO_6.[3,5] These results raise the question of whether large octahedral rotations are present in the cubic phases of these other compounds as well.

CONCLUSIONS

This investigation demonstrates for the first time a complete structural characterization of a series of polymorphs which result from a sequence of phase transitions in double-perovskite-based structures with noncooperative octahedral tilting. The remarkable feature of these phase transitions is a steplike decrease in the fraction of the AlF_6 octahedral units which are rotated over a large angle of ~45° on going from the low-temperature to high-temperature polymorphs. The fraction of rotated octahedra decreases from two-fifths in α-K_3AlF_6 to one-fifth in β-K_3AlF_6, one-sixth in γ-K_3AlF_6, and zero in δ-K_3AlF_6. Other octahedra in these structures undergo only relatively small tilts. The reduction in the number of AlF_6 octahedra which undergo large tilts also results in a systematic decrease in the coordination numbers of the K ions on the B-sites. In α-K_3AlF_6, three-fifths of these atoms are 8-coordinate and two-fifths are 7-coordinate. In β-K_3AlF_6, there are no longer any 8-coordinate B-site K atoms, but instead

four-fifths are 7-coordinate and one-fifth are 6-coordinate. Upon going to γ-K_3AlF_6, the coordination of the K atoms on the B-site is further reduced so that two-thirds are 7-coordinate and one-third are 6-fold coordinate. In the highest temperature δ-phase, all B-site cations have a coordination number of 6. This behavior results in a discontinuous nature of the phase transitions and is drastically different from octahedral tilting distortions in conventional perovskites, where the corner-sharing links between the octahedral units force them to behave cooperatively.

This study also shows an increase in the amount of structural disorder as the temperature is increased. The α-phase appears to be very crystalline, with all atoms having well-defined positions. In the β- and γ-phases it is suspected that many of the apparently untilted AlF_6 octahedra begin to undergo large-amplitude dynamic rotations. The highly tilted AlF_6 octahedra in the γ-phase also show disorder in the direction of their rotations. The average crystal structure of δ-K_3AlF_6 is cubic, but pair distribution function analysis shows that all AlF_6 octahedra undergo large uncorrelated rotations which are accompanied by off-center displacements of the K^+ ions on the A-sites. The average rotation of the AlF_6 octahedra in the δ-phase is about 10° at 400 °C.

■ ASSOCIATED CONTENT

Supporting Information. Tables showing the temperature dependence of the lattice parameters and unit cell volume in the temperature range of 125−145 °C as obtained from Pawley fits of the NPD patterns and lattice parameters of K_3AlF_6 at various temperatures as determined by Pawley fitting of the synchrotron X-ray powder diffraction data and figures showing the results of the Rietveld refinement of the XRD pattern of δ-K_3AlF_6, experimental PDF of δ-K_3AlF_6 and fit using the average long-range structure as a model, and fit of the PDF of δ-K_3AlF_6 from the RMC refinement. This material is available free of charge via the Internet at http://pubs.acs.org.

■ AUTHOR INFORMATION

Corresponding Author
*E-mail: gking@lanl.gov.

■ ACKNOWLEDGMENT

This work has benefited from the use of the NPDF at the Lujan Center at Los Alamos Neutron Science Center, funded by the Department of Energy (DOE) Office of Basic Energy Sciences. Los Alamos National Laboratory is operated by Los Alamos National Security LLC under DOE Contract DE-AC52 06NA25396. P.M.W. acknowledges financial support from the National Science Foundation (Award Number DMR-0907356). We thank Joan Siewenie and Thomas Proffen for assistance in collection of the total scattering data. We are grateful to the ESRF for providing the beamtime at ID31 and acknowledge Caroline Curfs for her kind help during the experiment. We thank Aziz Daoud-Aladine and Kevin Knight for assistance in collecting the NPD data on the HRPD. A.T. was funded by the Alexander von Humboldt Foundation.

■ REFERENCES

(1) Abakumov, A. M.; King, G.; Laurinavichute, V. K.; Rozova, M. G.; Woodward, P. M.; Antipov, E. V. *Inorg. Chem.* **2009**, *48*, 9336.
(2) Howard, C. J.; Kennedy, B. J.; Woodward, P. M. *Acta Crystallogr.* **2003**, *B59*, 463.
(3) Zuniga, F. J.; Tressaud, A.; Darriet, J. *J. Solid State Chem.* **2006**, *179*, 3607.
(4) Withers, R. L.; Welberry, T. R.; Brink, F. J.; Noren, L. *J. Solid State Chem.* **2003**, *170*, 211.
(5) King, G.; Abakumov, A. M.; Hadermann, J.; Alekseeva, A. M.; Rozova, M. G.; Perkisas, T.; Woodward, P. M.; Van Tendeloo, G.; Antipov, E. V. *Inorg. Chem.* **2010**, *49*, 6058.
(6) Stoger, B.; Weil, M.; Zobetz, E. *Z. Kristallogr.* **2010**, *225*, 125.
(7) Jeitschko, W.; Mons, H. A.; Rodewald, U. C.; Möller, M. H. *Z. Naturforsch.* **1998**, *53*, 31–36.
(8) Bramnik, K. G.; Miehe, G.; Ehrenberg, H.; Fuess, H.; Abakumov, A. M.; Shpanchenko, R. V.; Pomjakushin, V.Yu.; Balagurov, A. M. *J. Solid State Chem.* **2000**, *149*, 49–55.
(9) Tomaszewska, A.; Müller-Buschbaum, H. *Z. Anorg. Allg. Chem.* **1993**, *619*, 1738–1742.
(10) Abakumov, A. M.; Rossell, M. D.; Alekseeva, A. M.; Vassiliev, S. Y.; Mudrezova, S. N.; Van Tendeloo, G.; Antipov, E. V. *J. Solid State Chem.* **2006**, *176*, 421.
(11) Grjotheim, K.; Holm, J. L.; Mikhael, S. A. *Acta Chem. Scand.* **1973**, *27*, 1299.
(12) Steward, E. G.; Rooksby, H. P. *Acta Crystallogr.* **1953**, *6*, 49.
(13) *Topas Academic, General Profile and Structure Analysis Software for Powder Diffraction Data*; Bruker AXS: Karlsruhe, Germany, 2004.
(14) Petricek, V.; Dusek, M. *The Crystallographic Computing System JANA2000*; Institute of Physics: Praha, Czech Republic, 2000.
(15) Peterson, P. F.; Gutmann, M.; Proffen, Th.; Billinge, S. J. L. *J. Appl. Crystallogr.* **2000**, *33*, 1192.
(16) Tucker, M. G.; Keen, D. A.; Dove, M. T.; Goodwin, A. L.; Hui, Q. *J. Phys.: Condens. Matter* **2007**, *19*, 335218.
(17) Brown, I. D.; Altermatt, D. *Acta Crystallogr.* **1985**, *B41*, 244.
(18) Brown, I. D.; Dabkowski, A.; McCleary, A. *Acta Crystallogr.* **1997**, *B53*, 750.
(19) Hong, S.-T. *J. Solid State Chem.* **2007**, *180*, 3039.
(20) Zhou, Q.; Kennedy, B. J. *J. Solid State Chem.* **2004**, *177*, 654.